NGD Analysis of Defected Ground and SIW-Matched Structure

Taochen Gu, Fayu Wan, Junxiang Ge, Lalléchère Sébastien, Rahajandraibe Wenceslas, Rahajandraibe Wenceslas, Wenceslas Rahajandraibe, Ravelo Blaise

NGD Analysis of Defected Ground and SIW-Matched Structure

Fayu Wan, *Member*, *IEEE*, Taochen Gu, Junxiang Ge, Sébastien Lalléchère, *Member*, *IEEE*, Wenceslas Rahajandraibe, *Member*, *IEEE* and Blaise Ravelo, *Member*, *IEEE*

***Abstract*—An innovative design of bandpass (BP) negative group delay (NGD) passive circuit based on defect ground structure (DGS) is developed in the present paper. The NGD DGS topology is originally built with notched cells associated with self-matched substrate waveguide elements. The DGS design method is introduced as a function of the geometrical notched and substrate integrated waveguide via elements. Then, parametric analyses based on full wave 3-D electromagnetic S-parameter simulations were considered to investigate the influence of DGS physical size effects. The design method feasibility study is validated with fully distributed microstrip circuit prototype. Significant BP NGD function performances were validated with 3-D simulations and measurements with -1.69 ns NGD value around 2 GHz center frequency over 33.7 MHz NGD bandwidth with insertion loss better than 4 dB and reflection loss better than 40 dB.**

***Index Terms*—Defected ground structure (DGS), Design method, Bandpass negative group delay (BP NGD) function, Experimentation, Microstrip circuit.**

I. Introduction

FOLLOWING the traditional technique to increase the electronic and electrical system performance consists in the integration density increase and size shrinking. However, the electronic system confinement is naturally penalized by the electromagnetic compatibility (EMC) and interference (EMI) undesirable effects [1-4]. Against the undesirable PCB EMI and EMC problems, different geometrical solutions were deployed. Research work on EMC and EMI design is permanently ongoing against this technical electronic and electrical system design challenge. Based on the EMI field-circuit simulation, an optimization design of vehicle navigation system was introduced [1].

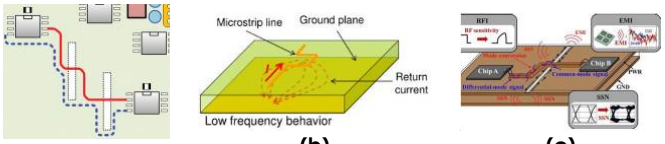

Fig. 1. EMI effects of DGS ((a) [5], (b) [6] and (c) [7]).

To predict these EMC and EMI effects, printed circuit board (PCB) level computation tools were investigated [2]. Computerized [3] and full-wave [4] simulations in EMC PCB level were proposed. The costs of the EMC and EMI issues constitute a major breakthrough for the PCB manufacturers. Therefore, the electronic PCB designers are continuously looking for the best technical solution without increasing the cost. And also, to alleviate the PCB EMIs, the proposal solution must guarantee that the design level of complexity does not increasing.

Among these solutions, our attention is bibliographically attracted to the deontological electronic ones consisting in modifying the paths of return current propagating through the ground plane as can be understood in Figs. 1 [5-7]. Such solutions were currently assigned as the defected ground structure (DGS) EMI reduction solutions [5-11]. This relevant and costless EMI solution candidate is generally applied to microstrip circuit designs as illustrated in Figs. 1 [5-7]. The DGS design solution is particularly efficient to suppress PCB level EM crosstalk [8-11]. An innovative GDS approach using irregularly-spaced vias connecting the PCB traces over a slotted ground plane is proposed in [8]. The effective of the DGS solution was verified to reduce radio frequencies and broadband EMIs from active PCBs [9-10]. The effectiveness of crosstalk suppression was validated from mode mismatch between spoof SPP microstrip transmission line (TL) [11]. In a high-speed (HS) PCBs, the effectiveness of DGS solution was demonstrated to mitigate simultaneous switching noise (SSN) and EMI reduction in [12].

Moreover, in addition to the EMI effect cancellation, the enormous sleeping potential of DGS need to be explored by the EMC, signal integrity (SI), RF and microwave design researchers. Under such a circumstance, we can point out that the DGS enables also to enhance the signal integrity (SI) performances [13-14] and suppression of microwave device harmonics [15]. In more general review, the DGS constitutes one of promising design solution and miniaturization

Manuscript received xxx xx, 2020; revised xxx xx, 2020; accepted xxx xx, 2020. Date of publication xxx xx, 2020.

This research work was supported in part by NSFC under Grant 61971230, and in part by Jiangsu Distinguished Professor program and Six Major Talents Summit of Jiangsu Province (2019-DZXX-022) and in part supported by the Startup Foundation for Introducing Talent of NUIST.

Fayu Wan, Taochen Gu, Junxiang Ge and Blaise Ravelo are with the Nanjing University of Information Science & Technology (NUIST), 210044 Nanjing, Jiangsu, China (e-mail: fayu.wan@nuist.edu.cn; 1448661697@qq.com; jxge@nuist.edu.cn. Corresponding author e-mail: blaise.ravelo@nuist.edu.cn).

Sébastien Lalléchère is with the Université Clermont Auvergne (UCA), CNRS, SIGMA Clermont, Institut Pascal, Aubière, France.
(email: sebastien.lallechere@uca.fr).

Wenceslas Rahajandraibe is with Aix-Marseille University, CNRS, University of Toulon, IM2NP UMR7334, Marseille, France
(email: wenceslas.rahajandraibe@im2np.fr).

minimizing the EMIs of various microwave passive circuits [15-25]. Because of these technical benefits, the DGSs have been extensively exploited to design microwave circuits. For example, the DGS circuits have an outstanding potential of integrability in different microwave devices as power dividers/combiners [15], filters [16-19], and antennas [20]. The extension of certain electronic function can also be exploited with the control of DGS parameters. By designing DGS resonator, a tunable band stop circuit was implemented by using reconfigurable dumbbell-shaped coplanar waveguide [21].

In addition to these classical microwave function designs, the DGS was also exploited to design the unfamiliar BP negative group delay (NGD) function [22-25]. It was found that the defected microstrip structures enable to design dual-band NGD circuits (NGDCs) operating between 3.46-3.58 GHz and 5.10-5.20 GHz [22]. Furthermore, compact NGD microstrip passive circuits with DGSs were designed [22-24]. However, the BP NGD performances of existing DGS microwave circuits are susceptible to be improved by playing on their geometry. For this reason, a novel design of DGS via elements is proposed in this paper by means of notched elements combined with substrate integrated waveguide.

Before the paper outline, it is worth to describe briefly the state-of-the-art on the unfamiliar BP NGD microstrip circuits [22-35]. Because of its intriguing counterintuitive aspect, the NGD existence was one of controversial topics for many microwave design researchers. The BP NGD function was understood in early 2000s with split ring resonator (SRR) based negative refractive index (NRI) metamaterial structure [26-27]. However, the NGD passive circuits were initially present more than 20 dB losses with important physical sizes [26-27]. Therefore, few research teams around the world were curiously attracted to the low and compact NGD circuit design in order to overcome this technical bottleneck [22-35]. Moreover, most of non-specialist microwave design engineers are still wondering about the NGD designability. One of the helpful basic NGD theory enabling to understand in easier way the design method was introduced by considering the Kramer-Koenig analogy between the linear circuit transfer function magnitude and group delay (GD) [35]. Subsequently, the concept of BP NGD function was defined which can be verified with all microwave NGD circuits [22-35]. An interesting microwave engineering was revealed on the fact that the BP NGD function can be designed with unlimited diverse topologies. The study, design and test of diverse NGD microwave topologies are still an open research area for future design, fabrication and test research engineers for the three following decades. For example, the BP NGD function was verified with absorptive bandstop filter [28], microwave signal interference technique [29], microwave transversal filter approach [30] and TL based microstrip circuits [31-34]. Innumerable topologies of microstrip NGD circuits (NGDCs) [22-35] were deployed in order to reduce to reach competitive compactness's.

Behind this progressive NGD design investigation, further research works were required about the design of NGD microwave circuits by illustrating the adequate characterization techniques required by RF and microwave standards. The novelty of the present paper compared to the NGD research work available in the literature [22-35] is the design consideration of substrate waveguide via and the circuit compactness. The substrate waveguide was exploited to design classical microwave function as filters [36-37], based on the authors' knowledge the present paper is the first-time investigation on the design of compact NGD circuit.

The paper is organized in four main sections. Section II describes the key fundamental definition and design methodology to familiarize to the BP NGD passive circuit design. Section III is focused on the design application of DGS-SIW circuit. The feasibility of the NGD design is investigated with parametric analyses with respect to the DGS notched element physical sizes. Section IV will validate the DGS NGD topology with experimentation of microstrip prototype. Then, Section V ends the paper with a conclusion.

II. Theoretical Specifications of BP NGD Performance

The present section defines the BP NGD function key specifications. The qualification of BP NGD performance will be defined from two-port circuit S-parameters. Then, the design methodology for NGD passive distributed circuit will be elaborated.

A. Theoretical Recall on GD Parameter

The two-port system of Fig. 2 represents a circuit black box. The present case of study associates the two-port symmetric microwave passive circuits.

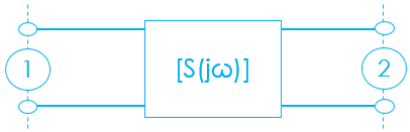

Fig. 2. Two-port black box system.

They can be theoretical modeled by an equivalent 2-D S-matrix written as:

$$[S(j\omega)] = \begin{bmatrix} S_{11}(j\omega) & S_{21}(j\omega) \\ S_{21}(j\omega) & S_{11}(j\omega) \end{bmatrix} \quad (1)$$

with $j\omega$ is the complex angular frequency variable.

The corresponding transmission coefficient phase is given by:

$$\varphi(\omega) = \arg\left[S_{21}(j\omega) \right]. \quad (2)$$

The specific parameter of the present study is expressed by the GD mathematically defined by:

$$GD(\omega) = \frac{-\partial\varphi(\omega)}{\partial\omega}. \quad (3)$$

For the case of BP NGD function, the equation:

$$GD(\omega) = 0 \quad (4)$$

should present two roots, ω_1 and ω_2, (we take $\omega_1<\omega_2$), which are named NGD cut-off frequencies.

B. Ideal Specifications of BP NGD Response

By analogy with all microwave function, the NGD one should be targeted to operate at specific NGD center frequency, ω_0 as introduced in Figs. 3. In the NGD bandwidth,

$\omega_1 < \omega < \omega_2$, given the desired values of positive reals, A<1 and B<1, the essential parameters of BP NGD function are:

- The reflection coefficient, $S_{11}=A$, as seen in Fig. 3(a),
- The transmission coefficient, $S_{21}=B$, as illustrated in Fig. 3(b),
- And as depicted in Fig. 2(c), the NGD value, $GD(\omega) = GD_0 < 0$,
- Over the NGD bandwidth:

$$\Delta\omega = \omega_2 - \omega_1 . \quad (5)$$

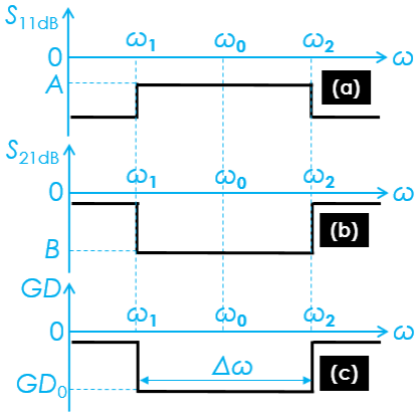

Fig. 3. Typical behaviors of BP NGD S-parameters: (a) reflection, (b) transmission coefficients and (c) GD.

C. Design Methodology of BP NGD Circuit

The BP NGD circuit design method is practically analog to the classical electronic circuits (filters, phase shifters, couplers, power dividers, …). The design can be organized in seven successive steps. The principal phases can be described as follows:

- The design process must begin with the desired BP NGD specifications as explained by the previous subsection.
- The minimal and maximal ranges of the physical parameters must be defined.
- After the 2-D or 3-D design of the passive circuit (in the present study limited to microstrip technology), the physical sizes of the widths, lengths and interspaces constituting the structure should be optimized.
- The BP NGD circuit final design should be followed by the fabrication.
- Then, the final stage will be BP NGD behavior validation tests of the prototype.

III. DGS Circuit Designing and Parametric Analyses with Respect to the Notched Element Physical Sizes

The present section is focused on the design description of notched element based DGS BP NGD circuit. It acts as a two-port passive circuit. Parametric analyses of GD and S-parameters will be discussed. All the computational results presented in this paper were obtained from 3-D electromagnetic full wave simulations. The present simulated results were run in the commercial tool environment of the microwave structure designer and simulator HFSS® from ANSYS® Electromagnetics Suite 19.0.0 which operates with solver Finite Element Method. The employed PC is equipped with a single-core processor Intel® CoreTM Intel(R) Core(TM) i5-8400 CPU @2.80GHz 2.81GHz and 16 GB physical RAM with 64-bits Windows 7.

A. Design of Notched Element Based DGS Circuit

Following the design flow elaborated in Fig. 3, the present subsection investigates the geometrical implementation of our DGS NGD proof-of-concept (POC). The BP NGD specifications targeted for the present circuit design are addressed in Table I. The POC DGS is mainly designed in microstrip topology by using a direct TL. Figs. 4 introduce the planar design of microstrip circuit geometrically designed with width, W, and length, L. The circuit is essentially composed of distributed elements without lumped element. As seen in top view of Fig. 4(a), the microstrip circuit is constituted by the direct TL presenting physical width, w_{port}. The direct TL was designed with characteristic impedance equal to the terminal load reference impedance, R_0=50 Ω.

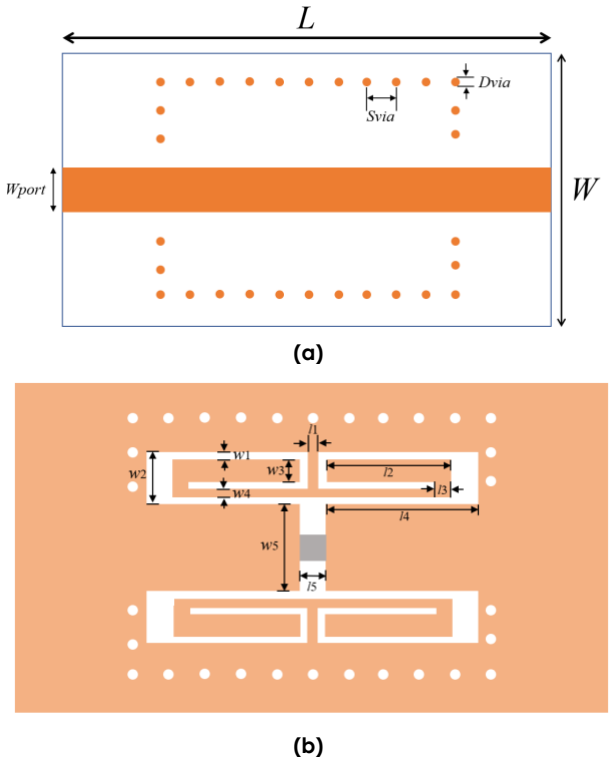

Fig. 4. DGS planar design: (a) top view of the overall circuit and (b) backside view of notched element.

TABLE I
TARGETED BP NGD SPECIFICATIONS

Parameter	DG_0	f_0	Δf	S_{11}	S_{21}
Value	-2 ns	2 GHz	40 MHz	-10 dB	-4 dB

As initial value, by denoting the substrate effective permittivity, ε_{reff}, and vacuum speed of light, c, the TL length was calculated via the formula:

$$L = \frac{c}{2 f_0 \sqrt{\varepsilon_{reff}}} . \quad (6)$$

As illustrated in Fig. 4(b), the DGS is constituted by bilateral side of interconnected holed and notched elements. The

notched elements present physical lengths, l_k, and widths, w_k, with k=1, …, 5. The notched element parameters were chosen in order to generate the BP NGD specifications targeted in Table I. As displayed in Fig. 4(b), in each side of the circuit, the notched element is surrounded in U-shape by aligned via hole with physical diameter, D_{via}, and interspaced, S_{via}. The POC NGD circuit was expected to operate under low-attenuation better than 4 dB and well access matching under return loss better than 10 dB.

B. DGS SIW Circuit Prototyping

The DGS circuit prototype was implemented on double side Copper metallized FR4-based substrate. The length and width physical sizes, l_k, and w_k, of the notched elements were optimized with HFSS® simulations in order to achieve the targeted BP NGD response specified previously in Table I. Fig. 5(a) and Fig. 5(b) display the HFSS® 3-D design view and photograph of top and back sides of the fabricated prototype with size, 19 × 34 mm. The final values of the POC circuit physical parameters are addressed in Table II.

For the better understanding the influence of each physical dimension on the BP NGD function, parametric analyses will be explored in the next paragraph.

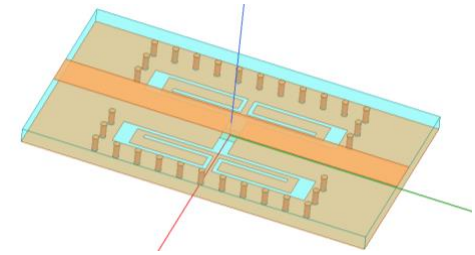

(a)

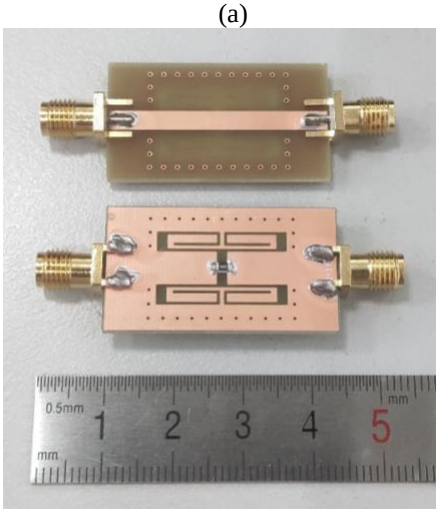

(b)

Fig. 5. (a) 3-D HFSS® design and (b) photograph of the fabricated DGS circuit prototype.

TABLE II
DGS CIRCUIT PARAMETERS AND SPECIFICATIONS

Components	*Description*	*Parameter*	*Value*
Dielectric substrate	Material	FR4	-
	Relative permittivity	ε_r	4.2
	Loss tangent	tan(δ)	0.02
	Thickness	h	1.5 mm
Metallization	Material	Copper (Cu)	-
	Thickness	t	35 µm
	Conductivity	σ	58 MS/m
DGS NGD circuit	Total length	L	34 mm
	Total width	W	19 mm
	Resistance	R	36 Ω
	Via diameter	D_{via}	0.6 mm
	Via interspace	S_{via}	1.5 mm
	Width	W_{port}	3.1 mm
		w_1	0.4 mm
		w_2	3 mm
		w_3	1.3 mm
		w_4	0.5 mm
		w_5	5 mm
	Length	l_1	0.6 mm
		l_2	7.3 mm
		l_3	0.92 mm
		l_4	8.75 mm
		l_5	1.5 mm

C. Parametric Analyses with Respect to the DGS Physical Sizes

The present parametric investigation is based on the S-parameter computation of the DGS structure introduced previously. The computations were carried out in the HFSS® environment withing the frequency bandwidth from 1.8 GHz to 2.2 GHz with 300 frequency samples. During the simulations, the considered notched element physical parameters were swept linearly. Then, the results will be discussed in the following paragraphs.

1) Parametric Analysis Versus l_1

The first parametric analysis was performed by varying l_1 from 0.4 mm to 1 mm and fixing all the other parameters in Table II. After simulations, we obtain the results mapped in Figs. 6. Fig. 6(a) illustrates that the BP NGD behavior is kept conserved despite the swept of l_1.

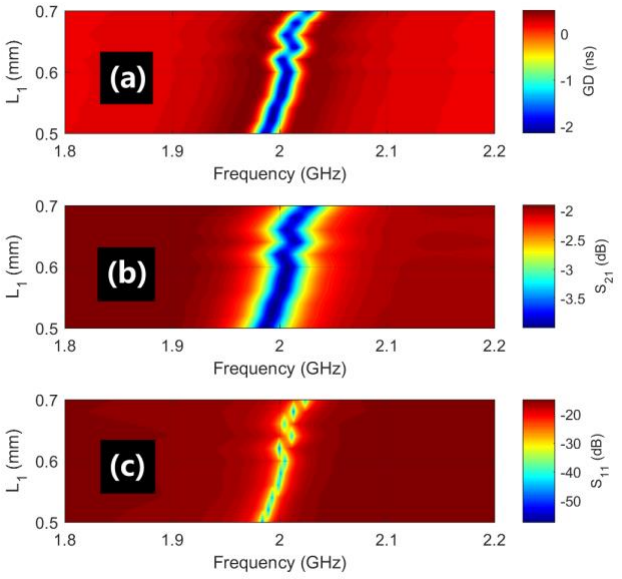

Fig. 6. Parametric simulated results versus d: (a) GD, (b) S_{11} and (c) S_{21}.

TABLE III
NGD SPECIFICATIONS VERSUS l_1

l_1 (mm)	Z (Ω)	f_0 (GHz)	$GD(f_0)$ (ns)	$S_{21}(f_0)$ (dB)	$S_{11}(f_0)$ (dB)
0.4	50.2	1.969	-2.22	-4.09	-44.4
0.6	49.9	2.007	-2.19	-4.07	-46.0
0.8	49.8	2.028	-1.94	-3.86	-34.7
1.0	49.7	2.064	-1.74	-3.78	-35.2

As witnessed by Table III, in the considered parametric range, the variation of l_1, influences remarkably the NGD center frequency, f_0, which increases from 1.969 GHz to 2.064 GHz. Moreover, the GD optimal value, $GD(f_0)$ present absolute value decreasing from about 2.22 ns down to 1.74 ns. As shown in Fig. 6(b), the transmission coefficient is increasing from -4.09 dB to -3.78 dB over reflection coefficient of Fig. 6(c) widely better than -10 dB.

2) Parametric Analysis Versus w_5

This second parametric analysis aims to investigate the influence of w_5. This later one was varied from 1.9 to 2.2 mm by fixing all the other ones as shown in Table II. Figs. 7 summarize the mappings of the GD, transmission and reflection coefficients. Table IV shows the BP NGD performances at different values of w_5. Fig. 7(a) illustrates the conservation of the DGS circuit BP NGD responses despite the variation of w_5.

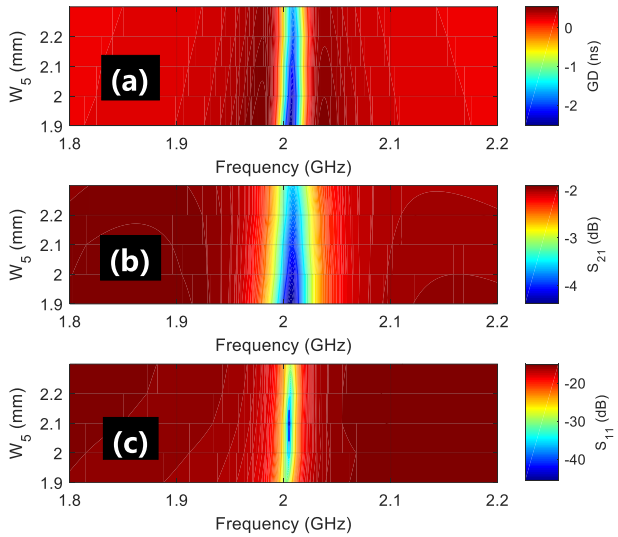

Fig. 7. Parametric simulated results versus L_2: (a) *GD*, (b) S_{11} and (c) S_{21}.

TABLE IV
NGD SPECIFICATIONS VERSUS w_5

w_5 (mm)	Z (Ω)	f_0 (GHz)	$GD(f_0)$ (ns)	$S_{21}(f_0)$ (dB)	$S_{11}(f_0)$ (dB)
4.8	49.9	2.006	-2.53	-4.38	-30.2
4.9	49.8	2.007	-2.32	-4.18	-36.3
5.0	49.9	2.007	-2.19	-4.07	-46.0
5.1	50.1	2.009	-1.87	-3.78	-34.4
5.2	49.8	2.009	-1.65	-3.59	-28.6

In this case, the NGD center frequency is slightly shifted with 3 MHz variation. The absolute value of $GD(f_0)$ is decreasing also from 2.53 ns to 1.65 ns. The transmission coefficient mapped in Fig. 7(b) is increasing from -4.38 dB to -3.59 dB.

3) Parametric Analysis Versus R

This last parametric analysis aims to investigate the influence of *R*. This later one was varied from 36 to 43 Ω by fixing all the other ones as shown in Table II. Figs. 8 plots the BP NGD responses of the DGS NGD circuit for the different values of *R*. Table V indicates the BP NGD specifications around the NGD center frequency, f_0. This later one variation can be considered as negligible under the variation of *R*. It can be understood from Fig. 8(a) that the resistor value influences the access matching. However, the transmission coefficient around the NGD center frequency presents less than 0.3 dB variation. More importantly, as explained by Fig. 8(c), the GD responses can be literally assumed as insensitive to the *R* variation.

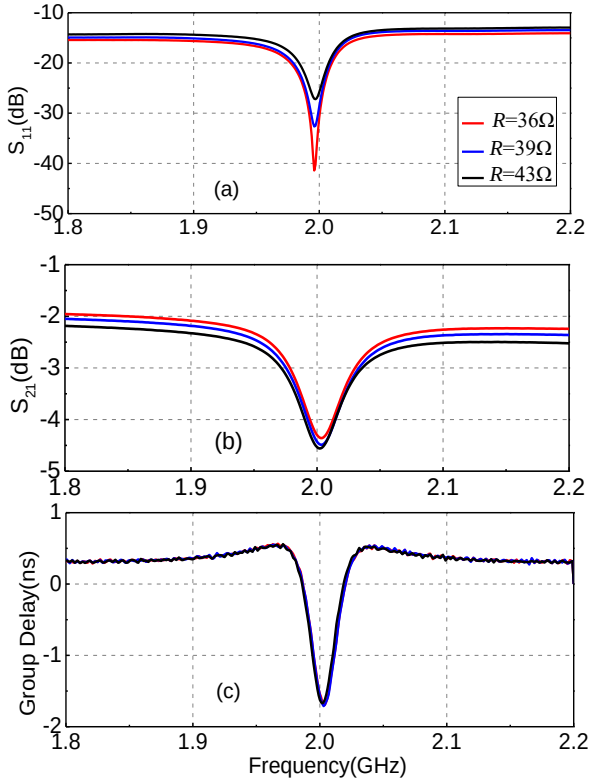

Fig. 8. Parametric simulated results versus *R*: (a) S_{11}, (b) S_{21} and (c) *GD*.

TABLE V
NGD SPECIFICATIONS VERSUS RESISTANCE, *R*

R (Ω)	f_0 (GHz)	$GD(f_0)$ (ns)	$S_{21}(f_0)$ (dB)	$S_{11}(f_0)$ (dB)
36	2.003	-1.69	-4.37	-41.5
39	2.003	-1.70	-4.49	-32.6
43	2.002	-1.67	-4.57	-27.2

IV. SIMULATED AND EXPERIMENTAL VALIDATION RESULTS

The BP NGD aspect of the DGS circuit prototype was investigated by comparisons of the full wave simulation and measurement. The experimented results will be discussed in the following subsection.

A. Test and Measurement of DGS NGD Circuit Prototype

Similar to classical microwave devices, the validation study was carried out via S-parameter measurement from 1.8 GHz to 2.2 GHz.

TABLE VI
SIMULATED AND EXPERIMENTED NGD PERFORMANCES

Validation Method	f_0 *(GHz)*	GD_n *(ns)*	*BW (MHz)*	S_{21} *(dB)*	S_{11} *(dB)*
Simulation	2.007	-2.19	28.7	-4.07	-46.0
Measurement	2.003	-1.69	33.7	-4.37	-41.5

TABLE VII
NGD PERFORMANCE COMPARISON

References	f_0 (GHz)	GD_n (ns)	*BW* (MHz)	S_{21} (dB)	S_{11} (dB)	*Size* (λ_g^2)
[13]	3.56	-4.24	62	-26.6	(*)	0.26×0.17
[14]	3.5	-3.8	100	-37.1	(*)	0.89×0.27
[21]	1	-1.5	370	-33	-28	0.78×0.06
[22]	1.79	-7.7	35	-8.6	-20	0.3×0.18
[23]	1.57	-8.75	60	-20.5	-32	0.39×0.19
Proposed one	2	-1.69	33.7	-4.37	-41	0.43×0.24

(*) No data in the origin references, simulation results indicate it is not better than -10 dB.

The experimental setup configuration with vector network analyzer (VNA) is shown in Fig. 9. The VNA is from Rohde & Schwarz® referenced ZNB 20 and specified by frequency band 100 kHz to 20 GHz. Figs. 10 show the comparisons between the simulated and measured results. The HFSS® computation speed was less than five minutes. As expected, these well-correlated results validate the BP NGD function of the notched element based DGS circuit. As plotted in Fig. 10(a), at the center frequency, f_0=2 GHz, the tested circuit present the NGD optimal simulated and measurement values, $GD(f_0)$, approximately -2.19 ns against -1.69 ns, respectively. The NGD bandwidth is approximately 33.7 MHz. As shown in Fig. 10(b) and in Fig. 10(c), the transmission coefficient is equal to -4.37 dB while the reflection coefficient is better than -41.5 dB within the NGD bandwidth. The differences between the simulated and experimental results are slight. Table VI summarizes the comparison of NGD performances from the simulation and measurement.

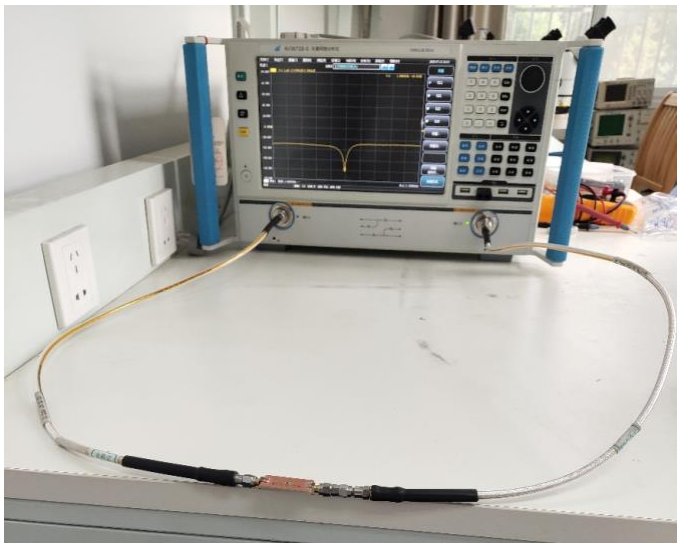

Fig. 9. Photograph of the DGS NGD circuit experimental setup.

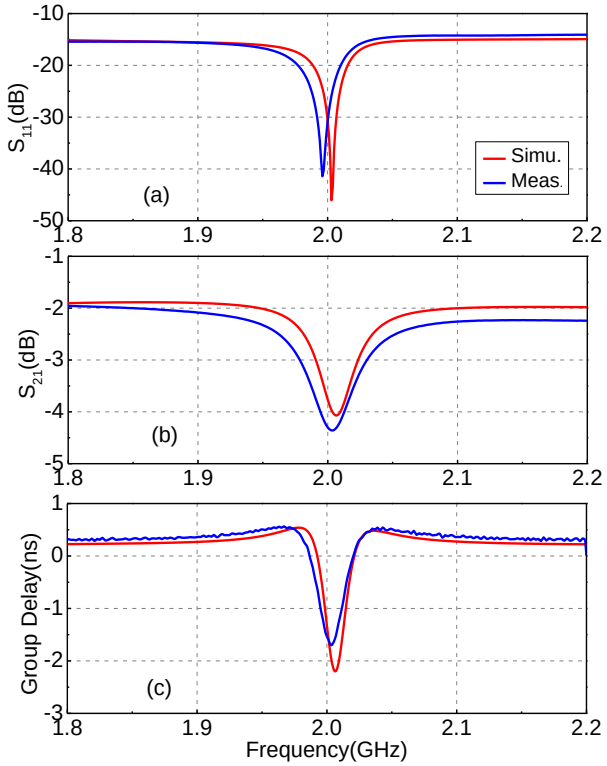

Fig. 10. Simulated and measured (a) GD, (b) reflection and (c) transmission coefficients of the fabricated circuit.

The following subsection will discuss the BP NGD performance comparisons between the developed DGS NGD result and the existing ones in the literature.

B. Discussion on Active Prototype NGD Performances Compared with the Literature

Table VII summarizes the comparison of NGD performance parameters with the literature NGD circuit [13-14,21-23]. Compared to the DGS NGD circuit introduced in [13-14,21-23], the DGS NGD circuit presented in this paper show the advantage in better transmission coefficient and reflection coefficient and relative compact size. As the DGS NGD circuit is simple and less influence parameter, it is easy to design and fabricate. The main circuit is designed at the back side of the PCB and the top size is only a TL, it is easy to be implemented in microwave circuit to equalize the delay.

V. Conclusion

An innovative design method of BP NGD DGS circuit implemented directly transmission TL associated with specific design of notched ground plane. The essential specifications of BP NGD functions are pedagogically defined. The design process of the DGS circuit is elaborated with the graphical design flow.

The feasibility study of the DGS BP NGD circuit is performed with the design description followed by parametric analyses in function of the key geometrical parameters of the notched elements. The fabricated circuit after optimization is described. The test results confirm an outstanding correlation between the BP NGD responses from simulation and measurement.

In the future, the DGS NGD topology is expected as a potential solution for microwave 5G-circuits against the size and NGD performances.

References

[1] H. Yang, X. Xiao, and H. Song, "Field-circuit simulation of electromagnetic interference and optimisation design in vehicle navigation system," IET Science, Measurement & Technology, vol. 14, no. 5, July 2020, pp. 552-556.

[2] B. Archambeault, C. Brench and S. Connor, "Review of printed-circuit-board level EMI/EMC issues and tools," IEEE Trans. Electromag. Comp., vol. 52, no. 2, 2010, pp. 455-461.

[3] X. Z. Wu, C. Zhang, S. F. Yang, and L. Q. Zhao, "Computerized Simulation of Board-Level EMC in High-Speed PCB," Advanced Materials Research, vol. 989-994, pp. 1977-1980, July 2014.

[1] V. Jandhyala, D. Gope, S. Chakraborty, R. Murugan, and S. Mukherjee, "Toward building full-system EMI verification and early design flows through full-wave electromagnetic simulation," Int. J. RF and Microwave Computer-Aided Engineering, vol. 22, no. 4, pp. 104-115, Jan. 2012.

[2] Available Online, Accessed August 2020, https://incompliancemag.com/article/slots-in-gnd-planes/

[3] Available Online, Accessed August 2020, https://www.slideserve.com/hua/design-guidelines-for-emc-of-components-powerpoint-ppt-presentation

[4] Available Online, Accessed August 2020, http://ntuemc.tw/theme/design/emc_01.jpg

[5] U. Choi, Y.-J. Kim, and Y.-S. Kim, "Crosstalk Reduction in Printed Circuit Boards Using Irregularly-Spaced Vias in a Guard Trace over a Slotted Ground Plane," Proc. of 2009 European Conference on Circuit Theory and Design, Antalya, Turkey, 23-27 Aug. 2009, pp. 794-797.

[6] A. Henridass, M. Sindhadevi, N. Karthik, M. G. N. Alsath, R. R. Kumar and K. Malathi, "Defective ground plane structure for broadband crosstalk reduction in PCBs," Proc. of 2012 Int. Conf. on Computing, Communication and Applications, Dindigul, Tamilnadu, India, 22-24 Feb. 2012, pp. 1-5.

[7] M. Sindhadevi, K. Malathi, A. Henridass, and A. K. Shrivastav, "Crosstalk reduction using defective ground plane structures in RF printed circuit boards," Arabian Journal for Science and Engineering, vol. 39, Feb. 2014, pp. 1107–1116.

[8] X. Gao, H. C. Zhang, P. H. He, Z. X. Wang, J. Lu, R. T. Yan, and T. J. Cui, "Crosstalk Suppression Based on Mode Mismatch Between Spoof SPP Transmission Line and Microstrip," IEEE Trans. Components Packaging and Manufacturing Technology, vol. 9, no. 11, Nov. 2019, pp. 2267-2275.

[9] M. M. Bait-Suwailam, and O. M. Ramahi, "Ultrawideband Mitigation of Simultaneous Switching Noise and EMI Reduction in High-Speed PCBs Using Complementary Split-Ring Resonators," IEEE Trans. Electromag. Comp., vol. 54, no. 2, Apr. 2012, pp. 389-396.

[10] S.-G. Kim, H. Kim, H.-D. Kang, and J.-G. Yook, "Signal Integrity Enhanced EBG Structure With a Ground Reinforced Trace," IEEE Trans. Components Packaging and Manufacturing Technology, vol. 33, no. 4, Oct. 2010, pp. 284-288.

[11] M. Sindhadevi, K. Malathi, A. Henridass, and A. K. Shrivastav, "Signal Integrity Performance Analysis of Mutual Coupling Reduction Techniques Using DGS in High Speed Printed Circuit Boards," Wireless Pers. Commun., vol. 94, pp. 3233–3249, June 2017.

[12] W. Duk-Jae and L. Taek-Kyung, "Suppression of harmonics in Wilkinson power divider using dual-band rejection by asymmetric DGS," IEEE Transactions on Microwave Theory and Techniques, vol. 53, no. 6, pp. 2139-2144, 2005.

[13] C. S. Kim, J. S. Park, D. Ahn, and J. B. Lim, "A novel 1-D periodic defected ground structure for planar circuits," IEEE Microw. Guided Wave Lett., vol. 10, no. 4, pp. 131–133, Apr. 2000.

[14] P. Jun-Seok, Y. Jun-Sik, and A. Dal, "A design of the novel coupled-line bandpass filter using defected ground structure with wide stopband performance," IEEE Transactions on Microwave Theory and Techniques, vol. 50, no. 9, pp. 2037-2043, 2002.

[15] L. Jong-Sik, K. Chul-Soo, D. Ahn, J. Yong-Chae, and N. Sangwook, "Design of low-pass filters using defected ground structure," IEEE Transactions on Microwave Theory and Techniques, vol. 53, no. 8, pp. 2539-2545, 2005.

[16] L. Zhou, Y. Ma, J. Shi, J. Chen, and W. Che, "Differential Dual-Band Bandpass Filter With Tunable Lower Band Using Embedded DGS Unit for Common-Mode Suppression," IEEE Transactions on Microwave Theory and Techniques, vol. 64, no. 12, pp. 4183-4191, 2016.

[17] C. Kumar, M. I. Pasha, and D. Guha, "Microstrip Patch With Nonproximal Symmetric Defected Ground Structure (DGS) for Improved Cross-Polarization Properties over Principal Radiation Planes," IEEE Antennas and Wireless Propagation Letters, vol. 14, pp. 1412-1414, 2015.

[18] A. M. E. Safwat, F. Podevin, P. Ferrari, and A. Vilcot, "Tunable Bandstop Defected Ground Structure Resonator Using Reconfigurable Dumbbell-Shaped Coplanar Waveguide," IEEE Transactions on Microwave Theory and Techniques, vol. 54, no. 9, pp. 3559-3564, 2006.

[19] G. Chaudhary, Y. Jeong and J. Lim, "Miniaturized Dual-Band Negative Group Delay Circuit Using Dual-Plane Defected Structures," IEEE Microwave and Wireless Components Letters, vol. 24, no. 8, pp. 521-523, Aug. 2014.

[20] G. Chaudhary, J. Jeong, P. Kim, Y. Jeong and J. Lim, "Compact negative group delay circuit using defected ground structure," 2013 Asia-Pacific Microwave Conference Proceedings (APMC), Seoul, 2013, pp. 22-24.

[21] R. Xian-Ke Gao, S.-P. Gao, H. M. Lee and E.-X. Liu, "Metamaterial-based common-mode noise filter with NGD effect for multilayer PCB," Negative Group Delay Devices: From concepts to applications, IET Materials, Circuit and Devices Series 43, Publisher Michael Faraday House, Hertfordshire, UK, November 2018, pp. 309-342.

[22] B. Ravelo, Negative Group Delay Devices: From concept to applications, IET Materials, Circuit and Devices Series 43, Publisher Michael Faraday House, UK, 2018.

[23] O. F. Siddiqui, M. Mojahedi and G. V. Eleftheriades, "Periodically Loaded Transmission Line With Effective Negative Refractive Index and Negative Group Velocity," IEEE Trans. Antennas Propagat., Vol. 51, No. 10, Oct. 2003, pp. 2619-2625.

[24] G. V. Eleftheriades, O. Siddiqui, and A. K. Iyer, "Transmission Line for Negative Refractive Index Media and Associated Implementations without Excess Resonators," IEEE Microw. Wireless Compon. Lett., Vol. 13, No. 2, pp. 51-53, Feb. 2003.

[25] L.-F. Qiu, L.-S. Wu, W.-Y. Yin, and J.-F. Mao, "Absorptive bandstop filter with prescribed negative group delay and bandwidth," IEEE Microw. Wireless Compon. Lett., vol. 27, no. 7, pp. 639-641, Jul. 2017.

[26] Z. Wang, Y. Cao, T. Shao, S. Fang and Y. Liu, "A Negative Group Delay Microwave Circuit Based on Signal Interference Techniques," IEEE Microw. Wireless Compon. Lett., vol. 28, no. 4, pp. 290-292, Apr. 2018.

[27] C.-T.-M. Wu and T. Itoh, "Maximally flat negative group-delay circuit: A microwave transversal filter approach," IEEE Trans. Microw. Theory Techn., vol. 62, no. 6, pp. 1330-1342, Jun. 2014.

[28] G. Liu and J. Xu, "Compact transmission-type negative group delay circuit with low attenuation," Electron. Lett., vol. 53, no. 7, pp. 476-478, Mar. 2017.

[29] T. Shao, Z. Wang, S. Fang, H. Liu, and S. Fu, "A compact transmission line self-matched negative group delay microwave circuit," IEEE Access, vol. 5. pp. 22836-22843, Oct. 2017.

[30] T. Shao, S. Fang, Z. Wang and H. Liu, "A Compact Dual-Band Negative Group Delay Microwave Circuit," Radio Engineering, vol. 27, no. 4, pp. 1070-1076, Dec. 2018.

[31] X. Zhou, B. Li, N. Li, B. Ravelo, X. Hu, Q. Ji,F. Wan and G. Fontgalland, "Analytical Design of Dual-Band Negative Group Delay Circuit with Multi-Coupled Lines," IEEE Access, Vol. 8, No. 1, Apr. 2020, pp. 72749-72756.

[32] B. Ravelo, "On the low-pass, high-pass, bandpass and stop-band NGD RF passive circuits," URSI Radio Science Bulletin, Vol. 2017, No. 363, Dec. 2017, pp. 10-27.

[33] M. Esmaeili and J. Bornemann, "Novel Tunable Bandstop Resonators in SIW Technology and Their Application to a Dual-Bandstop Filter with One Tunable Stopband," IEEE Microw. Wireless Compon. Lett., vol. 27, no. 1, 2017, pp. 40–42.

[34] A. P. Saghati, A. P. Saghati and K. Entesari, "Ultra-Miniature SIW Cavity Resonators and Filters," IEEE Trans. Microw. Theory Techn., vol. 63, no. 12, 2015, pp. 4329–4340.